2020

Magnetic and magnetocaloric properties of Fe2Ta thin films

S. Shaji

Nikhil R. Mucha

P. Giri

C. Binek

D. Kumar

AIP Advances

Magnetic and magnetocaloric properties of Fe_2Ta thin films

Cite as: AIP Advances **10**, 025222 (2020); https://doi.org/10.1063/1.5134796
Submitted: 04 November 2019 . Accepted: 23 January 2020 . Published Online: 19 February 2020

S. Shaji, Nikhil. R. Mucha, P. Giri, C. Binek, and D. Kumar

Magnetic and magnetocaloric properties of Fe_2Ta thin films

Cite as: AIP Advances 10, 025222 (2020); doi: 10.1063/1.5134796
Submitted: 4 November 2019 • Accepted: 23 January 2020 •
Published Online: 19 February 2020

View Online Export Citation CrossMark

S. Shaji,[1] Nikhil. R. Mucha,[1] P. Giri,[2] C. Binek,[2] and D. Kumar[1,a)]

AFFILIATIONS

[1]Department of Mechanical Engineering, North Carolina A & T State University, Greensboro, North Carolina 27411, USA
[2]Department of Physics and Astronomy, University of Nebraska-Lincoln, Lincoln, Nebraska 68588, USA

[a)]**Author to whom correspondence should be addressed:** dkumar@ncat.edu. **Tel.:** 001-336-285-3227.

ABSTRACT

A magnetocaloric effect (MCE) on rare-earth free Fe_2Ta thin films is reported. The structural characterizations carried out using x-ray diffraction and transmission electron microscopy have indicated the formation of a Laves phase in the Fe_2Ta film in a $MgZn_2$ type crystal structure. Applying the Maxwell relation to the magnetization (M) vs temperature (T) curves at various fields (H), $\partial M/\partial T$ vs H curves were integrated to indirectly obtain quantitative information about the isothermal entropy change. A positive MCE with an entropy change as high as 6.9 J/K m^3 at 10 K and a negative MCE with an entropy change as high as −2.0 J/K m^3 at 300 K were observed for the magnetic fields in the range of 0.05–0.5 T. The temperatures at which a crossover in the sign of the entropy change takes place were found to be a function of the field applied that ranged from 121 K at 5000 Oe to 159 K at 1000 Oe. The coexistence of the positive and negative MCE is attributed to a paramagnetic–antiferromagnetic transition in the Fe_2Ta system.

There is a strong need to develop new material systems and technologies with efficient refrigeration capability to reduce energy consumption without leaving any footprint on the environment.[1–5] Magnetic refrigeration is a good candidate to achieve this goal due to its high energy efficiency potential. The current refrigeration is almost entirely based on the gas compression/expansion refrigeration cycle.[1,3,5,6] The magnetic refrigeration process is based on the magnetocaloric effect (MCE).[4,7–9] It is a magneto-thermodynamic phenomenon in which an adiabatic change in temperature of a MC material is caused by exposing the thermally isolated material to a magnetic field.[5,8,10,11] According to the Department of Energy, heating, ventilation, and cooling (HVAC) accounts for ~36% of electricity consumed by US households. Central air-conditioning and refrigeration accounted for ~30% of the total electricity used in homes. Therefore, there is a clear consensus that improved refrigeration technology is of major importance and potentially a large part of the solution to the energy crisis.

In this work, we report the observation of an MCE in pulsed laser deposited rare-earth free magnetic $Fe_{67}Ta_{33}$ alloy thin films, where subscript numbers 67 and 33 indicate the chemical composition of the alloy in atomic percentage, which is an average value of 25 sites on the Fe–Ta thin film obtained using x-ray fluorescence (XRF) analysis. The corresponding chemical formula of the alloy is Fe_2Ta. Fe_2Ta alloy thin films were deposited at 300–400 °C on c-plane sapphire (0001) substrates using a composite Fe–Ta target and a pulsed laser deposition (PLD) method.[12–14] The laser was operated at a pulse rate of 10 Hz with an energy of 380 mJ/pulse. The films were grown in vacuum of ~5×10^{-7} Torr. The selection of the Fe_2Ta composition is based on its existence as a single phase in the Fe–Ta phase diagram.[15,16] According to the Fe–Ta phase diagram, the Fe–Ta system exists as a single phase in two composition windows: the first single phase is below 2.5 at. %, and the second single phase is around 28–35 at. %. While the first single phase retains the structure of fcc iron, the increasing doping level of Ta results in the formation of a single phase Laves phase around 28–35 at. %. In our previous publication,[17] we have provided results on the magnetic and transport properties of 10 wt. % doped Fe–Ta thin films, i.e., $Fe_{90}Ta_{10}$. In terms of atomic percentage, this composition is expressed as $Fe_{96.7}Ta_{3.3}$ with a chemical formula of $Fe_{29}Ta$. The level of Ta doping is much higher in the present work, but the phase is

still a single phase. The resulting Fe_2Ta thin films have a Laves phase $MgZn_2$ type crystal structure and show antiferromagnetic (AFM) properties. The Laves phase C14 hexagonal crystal structure of F_2Ta with a radius ratio, r_{Ta}/r_{Fe} = 1.7, is shown in the inset of Fig. 1. The number of Fe and Ta atoms per unit cell is eight (one vertex and one edge atom and six inside the cell atoms) and four (inside the cell), respectively, making four Fe_2Ta formula units per unit cell, which are used in the calculation of the net magnetic moment of the Fe_2Ta material system in the subsequent section.

It is interesting to note that there is a striking similarity between the phase diagrams of Fe–Ta and Fe–C systems.[15,16,18,19] However, the Fe–Ta alloy system is considered a very good alternative candidate to the Fe–C system as its mechanical hardness is ranked very high among materials known with the highest hardness.[20,21] The added advantage of the Fe_2Ta system is the possession of interesting magnetic[17] and magnetocaloric properties. Most of the work on the MCE has focused on materials containing rare-earth elements[1,6,22–25] since the entropy change scales with magnetic moment per atom which is high for rare earth elements.[26,27] With supply chain and related price stability issues, efforts are being made to explore magnetocaloric materials that do not contain rare-earth elements.[4,5]

The XRD pattern of a typical Fe–Ta film grown on sapphire substrates at 300 °C is shown in Fig. 1. The matching of the XRD (110), (211), and (220) peaks with the JCPDS data confirms the formation of Fe_2Ta films in the Laves phase with a C14 $MgZn_2$ type of crystal structure.[12] The full width at half maximum (FWHM) of 0.08° for the (hkl-110) peak calculated from the rocking curve indicates the highly crystalline nature of the film. The magnetic properties of Fe_2Ta films were investigated using the vibrating sample magnetometer (VSM) feature of a Quantum Design physical property measurement system (PPMS). The magnetic field was applied along the surface of the film during magnetization (M) vs temperature (T) measurements. Constant field M–T curves recorded for the Fe_2Ta film at various magnetic field strengths are shown in Fig. 2(a). The figure shows that as temperature decreases, there is a distinct peak in the magnetization in all the fields of measurements. As marked in the figure, the temperature where the maximum magnetization takes place is dependent on the field applied. The inverse susceptibility, obtained from the MT curves using $\chi^{-1} = \frac{H}{M}$, is plotted in Fig. 2(b). χ^{-1} is linear, which fits well to the Curie–Weiss law,

$$\chi^{-1} = \frac{T-\theta}{C}, \tag{1}$$

where C is the Curie constant, and θ is the Weiss temperature. The fitting is shown by a solid line on each curve. The values of C and θ, obtained from the fits, are listed in Table I. The goodness of the fit is evident from the low normalized chi

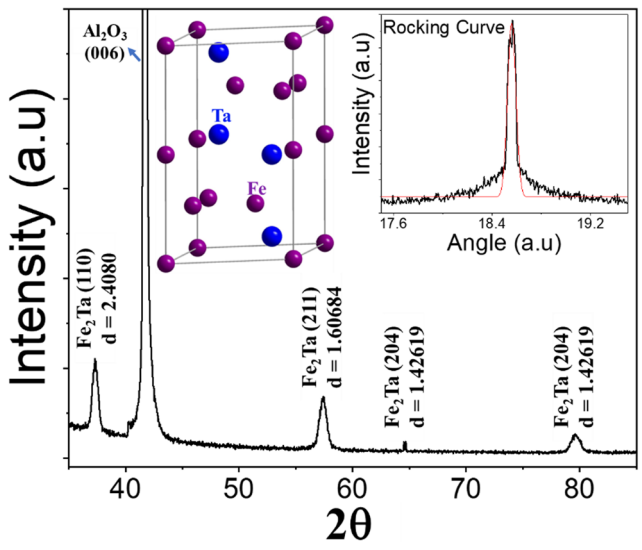

FIG. 1. XRD of a Fe_2Ta thin film grown on a sapphire substrate at 300 °C. The inset shows the unit cell crystal structure of F_2Ta and the rocking curve of the Fe_2Ta (110) peak.

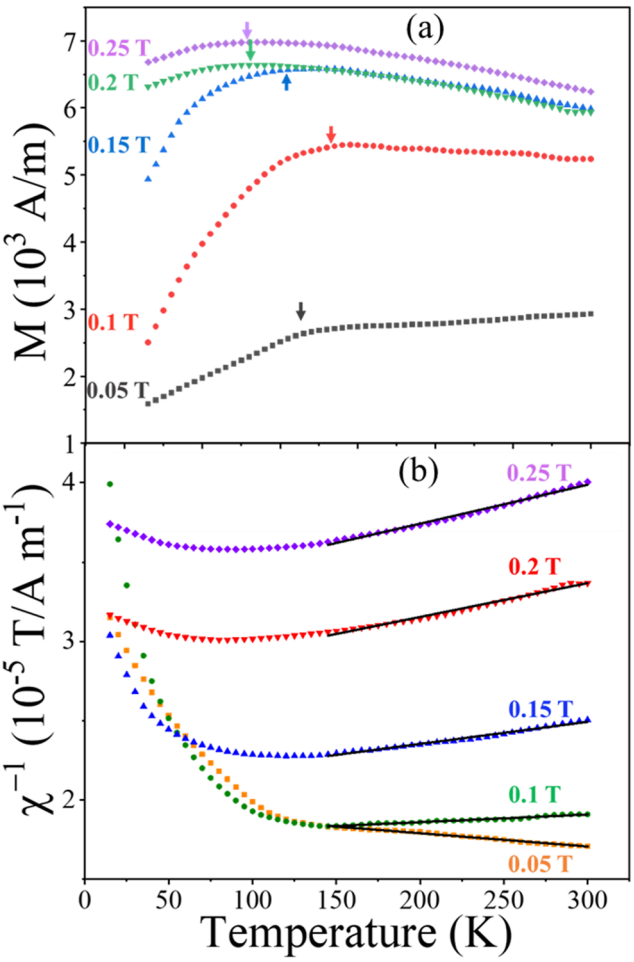

FIG. 2. (a) Zero field cooled magnetization (M) as a function of temperature at several fields for a Fe_2Ta thin film grown on a sapphire substrate and (b) inverse susceptibility (χ^{-1}) plotted against temperature. The solid line is the fit to the equation $\chi^{-1} = (T - \theta)/C$, where C is the Curie constant, and θ is the Weiss temperature.

TABLE I. Values of the square of the correlation coefficient (R^2), normalized chi square (χ^2), and the best-fit coefficients—the Curie constant (C) and θ.

Field (T)	R^2	Normalized χ^2	C $\left(\frac{KA}{Tm}\right)$, (from the fit)	C $\left(\frac{KA}{Tm}\right)$, (calculated)	Theta, θ
0.05	0.987	6.4×10^{-6}	-12×10^7	1.3×10^7	2342.5
0.1	0.972	4.4×10^{-6}	21×10^7	1.2×10^7	−3658.3
0.15	0.986	11.3×10^{-6}	7.2×10^7	1.0×10^7	−1489.8
0.2	0.987	13.8×10^{-6}	4.7×10^7	0.7×10^7	−1275.1
0.25	0.991	8.7×10^{-6}	4.1×10^7	0.6×10^7	−1335.5

square (χ^2) values and close-to-unity values of the square of the correlation coefficient, R^2 (Table I). Normalized χ^2 is defined as $1/(N - nfit) \sum_{i=1}^{N} \left[\left(\rho^i_{raw} - \rho^i_{fit}\right)^2/\left(\rho^i_{fit}\right)^2\right]$, where N is the number of data points (=32), n_{fit} is the number of fitted parameters (=2), ρ_{raw} is the raw data, and ρ_{fit} is the best fitted data. The advantage of using normalized χ^2 is that we can immediately compare it with the experimental accuracy of our measurements such as magnetization and conclude about the goodness of the fit to a model/formula.[28–30] The Curie constant values obtained from the fit also match well with the Curie constant values calculated using the experimental data using the expression $C = \frac{MT}{B}$. The increase in the susceptibility above the Néel temperature (T_N) leads to negative values of θ, suggesting AFM interactions at low temperatures in the Fe_2Ta films. It should be noted that the Curie–Weiss temperature and critical temperature are similar in ferromagnets. In antiferromagnets, however, this is not the case, and there is often even a qualitative sign difference between the antiferromagnetic order temperature and the Curie–Weiss temperature. We interpret the results of our fits as additional confirmation that, indeed, as indicated by the temperature dependence of the entropy change, the system undergoes a magnetic phase transition into an antiferromagnetic phase. Assuming the net magnetic moment arising only from Fe, the net magnetic moment of Fe_2Ta per formula unit is 0.014 μ_B, which is almost two orders of magnitude smaller than the magnetic moment of Fe per atom (2.14 μ_B). The magnetic moment per formula unit of Fe_2Ta is calculated using $m_{Fe2Ta} = (m_{sat}/\rho_{Fe2Ta})/m_{Bohr}$, where m_{Fe2Ta} is the magnetic moment of Fe_2Ta in terms of a Bohr magneton, m_{sat} is the saturation magnetization of Fe_2Ta in A/m, ρ is the molecular density, and $m_{Bohr} = 9.27\ 10^{-24}\ Am^2$.

The magnetocaloric cooling characteristics of Fe–Ta thin films were investigated using a magnetization based indirect measurement.[1,7,11,13,31] A more common way to characterize magnetocaloric materials is carried out by static magnetometry with the help of Maxwell's relation.[32] In Maxwell's relation, the magnetic field is changed while the material is thermally connected to a heat sink/reservoir and therefore remains at a constant temperature. The indirect measurement of the MCE, applied in the present work, is based on determining the entropy change in the material solely based on magnetic measurements and thermodynamic arguments via Maxwell's relation.[1,2,7,13,33] From the classical theory of thermodynamics, the entropy change while changing magnetic field is given by[7,24,31,34]

$$\Delta S = S(T, H_f) - S(T, H_i), \tag{2}$$

$$= \mu_0 V \int_{H_i}^{H_f} \left(\frac{\partial S}{\partial H}\right)_T dH. \tag{3}$$

By using Maxwell's relation,[5,13,35]

$$\left(\frac{\partial S}{\partial H}\right)_T = \left(\frac{\partial M}{\partial T}\right)_H. \tag{4}$$

Substituting Eq. (4) into Eq. (3) yields

$$\Delta S = \mu_0 V \int_{H_i}^{H_f} \left(\frac{\partial M}{\partial T}\right)_H dH, \tag{5}$$

where μ_0 is the vacuum permeability, V is the volume of the material, H_i and H_f represent the initial (typically zero) and final applied magnetic field,[36] ΔS is the magnetic field induced isothermal entropy change which can be taken to characterize the refrigerant capacity (RC) of the magnetic materials,[8,24,25,37]

$$RC = -\int_{T_1}^{T_2} \Delta S(T) dT. \tag{6}$$

These M–T curves were then differentiated to obtain the change in magnetization with respect to temperature over the entire magnetic field range (Fig. 3). The solid lines in this figure are mere guides to the eye. The *dM/dT* data were then integrated via Eq. (5) over the

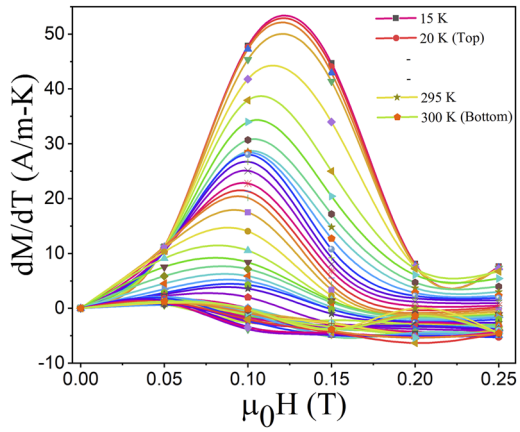

FIG. 3. dM/dT plots as a function of applied field ($\mu_0 H$) for a Fe_2Ta thin film sample.

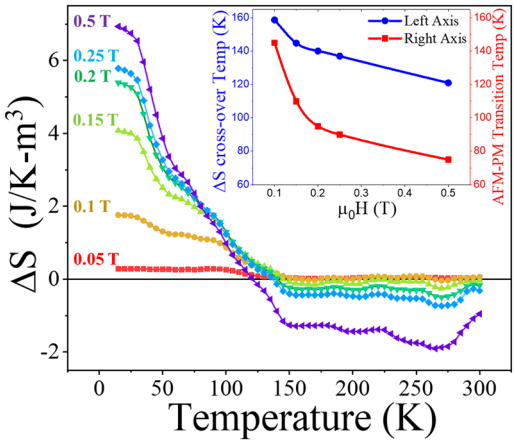

FIG. 4. Change in the entropy (ΔS) a function of temperature for a Fe_2Ta thin film sample. Inset: positive to negative crossover temperature (left y-axis) and magnetic phase transition temperature (right y-axis) plotted against applied field.

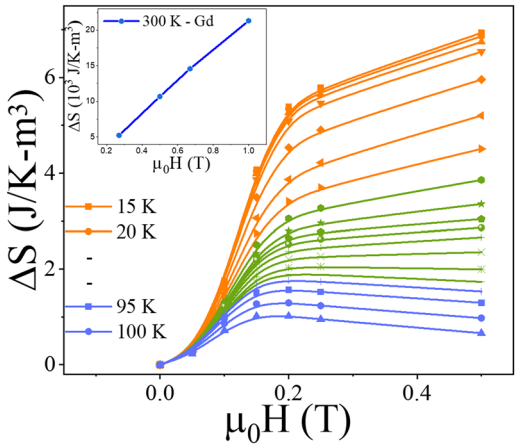

FIG. 5. Change in the entropy (ΔS) as a function of applied field (μ_0H) at temperatures indicated in the figure. For comparison, ΔS vs μ_0H for a gadolinium sample at 300 K is plotted in the inset.[42]

field range to estimate the change in entropy as a function of field. The entropy changes per unit volume as a function of temperature and field for the same sample are shown in Fig. 4. It can be noted from Fig. 4 that there is a sign reversal in the entropy change that is a function of temperature and field applied. Except for the field of 0.05 T, which has a positive MCE in the entire temperature range of the study, the sign of entropy change for all other fields is positive below 120 K. The temperatures corresponding to the crossover from the positive to negative MCE are plotted as a function of field applied, as shown in the inset of Fig. 4. As seen in the inset figure, the crossover temperature increases as the field is decreased, varying from 121 K at 5000 Oe to 159 K at 1000 Oe. In the same inset, we have also plotted the AFM to paramagnetic (PM) transition temperatures, recorded from the respective M–T curves, as a function of the applied field. The positive to negative MCE crossover temperature appears to be correlated with the AFM to PM transition temperature that could be used to suggest that the sign reversal in the entropy change is associated with the magnetic phase transition from an AFM to PM state. A coexistence of the positive and negative MCE, the sign and magnitude of which are controlled by the magnitude of the field, has been observed in the past in other materials.[38–40] A combination of direct and inverse MCE has also been observed for other bulk materials that undergo several different magnetic transitions.[41]

The change in volume entropy is plotted as a function of field in Fig. 5 at many temperatures below which the MCE is positive. We have also plotted the literature values of the volume entropy change for Gd as an inset in Fig. 5 for comparison purpose.[42] Obviously, the volume specific entropy changes are small in comparison with Gd and many other existing magnetocaloric material.[43] However, the entropy change in Fe_2Ta thin films reaches a saturation-type of feature, as shown in Fig. 5, at small fields (~0.2 T) that are significantly lower than the magnetic fields generally used to saturate the MCE. Besides, we can still use the indirect MCE in the Fe_2Ta films to characterize the material such as finding its temperature dependence of the heat capacity by combining the magnetometry with the direct measurements.

In conclusion, Fe_2Ta thin films have been grown *in situ* in a $MgZn_2$ type lattice structure that possesses AFM characteristics at lower temperatures. The AFM characteristics were confirmed by fitting the temperature dependent inverse susceptibility data to the Curie–Weiss equation, Eq. (1). The values of the Curie constant obtained from the fit match well with those calculated using the experimental data. A positive MCE with an entropy change of ~6.8 J/K m^3 and a negative MCE with an entropy change of ~−2.0 J/K m^3 for the magnetic field in the range of 0.05–0.5 T have been observed at 10 K and room temperature, respectively. A more systematic work on the optimization of the level of dopants seems a logical task that is needed to develop a Fe–Ta alloy system with a better MCE.

This work was supported by the NSF through the Nebraska Materials Research Science and Engineering Center (MRSEC), Grant No. DMR-1420645.

REFERENCES

[1]C. W. Miller, D. V. Williams, N. S. Bingham, and H. Srikanth, J. Appl. Phys. **107**(9), 09A903 (2010).
[2]V. Recarte, J. I. Pérez-Landazábal, V. Sánchez-Alárcos, V. A. Chernenko, and M. Ohtsuka, Appl. Phys. Lett. **95**(14), 141908 (2009).
[3]M. A. Hamad, J. Supercond. Novel Magn. **27**(1), 263–267 (2014).
[4]O. Tegus, E. Brück, K. H. J. Buschow, and F. R. de Boer, Nature **415**(6868), 150–152 (2002).
[5]E. Brück, O. Tegus, X. W. Li, F. R. de Boer, and K. H. J. Buschow, Physica B **327**(2), 431–437 (2003).
[6]Y. Hu, Z. Li, B. Yang, S. Qian, W. Gan, Y. Gong, Y. Li, D. Zhao, J. Liu, X. Zhao, L. Zuo, D. Wang, and Y. Du, APL Mater. **5**(4), 046103 (2017).
[7]V. K. Pecharsky and K. A. Gschneidner, Jr., J. Magn. Magn. Mater. **200**(1), 44–56 (1999).
[8]K. A. Gschneidner, Jr., V. K. Pecharsky, A. O. Pecharsky, and C. B. Zimm, Mater. Sci. Forum **315**, 69–76 (1999).
[9]K. A. Gschneidner, Jr. and V. K. Pecharsky, J. Appl. Phys. **85**(8), 5365–5368 (1999).
[10]M. Venkat Narayana, G. Kotnana, and S. N. Jammalamadaka, J. Alloys Compd. **683**(Supplement C), 56–61 (2016).

[11] B. Yu, Q. Gao, B. Zhang, X. Meng, and Z. Chen, Int. J. Refrig. **26**(6), 622–636 (2003).
[12] M. Roy, N. R. Mucha, R. G. Ponnam, P. Jaipan, O. Scott-Emuakpor, S. Yarmolenko, A. K. Majumdar, and D. Kumar, Thin Solid Films **681**, 1–5 (2019).
[13] X. Moya, L. E. Hueso, F. Maccherozzi, A. I. Tovstolytkin, D. I. Podyalovskii, C. Ducati, L. C. Phillips, M. Ghidini, O. Hovorka, A. Berger, M. E. Vickers, E. Defay, S. S. Dhesi, and N. D. Mathur, Nat. Mater. **12**, 52 (2012).
[14] S. Shaji, N. R. Mucha, S. Fialkova, and D. Kumar, Data Brief **27**, 104714 (2019).
[15] L. Swartzendruber and E. Paul, J. Phase Equilib. **7**(3), 254–259 (1986).
[16] R. H. Jones, V. Zackay, and E. Parker, Metall. Mater. Trans. B **3**(11), 2835–2842 (1972).
[17] S. Shaji, N. R. Mucha, A. K. Majumdar, C. Binek, A. Kebede, and D. Kumar, J. Magn. Magn. Mater. **489**, 165446 (2019).
[18] J. Chipman, Metall. Mater. Trans. B **3**(1), 55–64 (1972).
[19] O. T. Lord, M. J. Walter, R. Dasgupta, D. Walker, and S. M. Clark, Earth Planet. Sci. Lett. **284**(1), 157–167 (2009).
[20] P. Sharma, H. Kimura, and A. Inoue, J. Appl. Phys. **100**(8), 083902 (2006).
[21] A. Inoue, B. Shen, H. Koshiba, H. Kato, and A. R. Yavari, Nat. Mater. **2**(10), 661–663 (2003).
[22] V. V. Khovaylo, V. V. Rodionova, S. N. Shevyrtalov, and V. Novosad, Phys. Status Solidi (b) **251**(10), 2104–2113 (2014).
[23] V. K. Pecharsky and K. A. G., Jr., Appl. Phys. Lett. **70**(24), 3299–3301 (1997).
[24] J. Du, Q. Zheng, Y. Li, Q. Zhang, D. Li, and Z. Zhang, J. Appl. Phys. **103**(2), 023918 (2008).
[25] L. Li, Y. Yuan, Y. Qi, Q. Wang, and S. Zhou, Mater. Res. Lett. **6**(1), 67–71 (2018).
[26] S. Roy, N. Khan, and P. Mandal, APL Mater. **4**(2), 026102 (2016).
[27] A. Waske, E. Lovell, A. Funk, K. Sellschopp, A. Rack, L. Giebeler, P. F. Gostin, S. Fähler, and L. F. Cohen, APL Mater. **4**(10), 106101 (2016).
[28] S. Chakraborty and A. Majumdar, Phys. Rev. B **53**(10), 6235 (1996).
[29] T. Nath, N. Sudhakar, E. McNiff, and A. Majumdar, Phys. Rev. B **55**(18), 12389 (1997).
[30] D. Kumar, J. Sankar, J. Narayan, R. K. Singh, and A. K. Majumdar, Phys. Rev. B **65**(9) (2002).
[31] T. Hashimoto, T. Numasawa, M. Shino, and T. Okada, Cryogenics **21**(11), 647–653 (1981).
[32] C. W. Miller, D. D. Belyea, and B. J. Kirby, J. Vac. Sci. Technol. A **32** (4), 040802 (2014).
[33] S. Hariharan and J. Gass, Rev. Adv. Mater. Sci **10**(5), 398–402 (2005).
[34] M. Zaidi, J. Dhahri, I. Zeydi, T. Alharbi, and H. Belmabrouk, RSC Adv. **7**(69), 43590–43599 (2017).
[35] P. Poddar, J. Gass, D. J. Rebar, S. Srinath, H. Srikanth, S. A. Morrison, and E. E. Carpenter, J. Magn. Magn. Mater. **307**(2), 227–231 (2006).
[36] C. Binek and V. Burobina, Appl. Phys. Lett. **102**(3), 031915 (2013).
[37] N. Bingham, M. Phan, H. Srikanth, M. Torija, and C. Leighton, J. Appl. Phys. **106**(2), 023909 (2009).
[38] V. Franco, K. R. Pirota, V. M. Prida, A. M. J. Neto, A. Conde, M. Knobel, B. Hernando, and M. Vazquez, Phys. Rev. B **77**(10), 104434 (2008).
[39] S. Aksoy, T. Krenke, M. Acet, E. F. Wassermann, X. Moya, L. Mañosa, and A. Planes, Appl. Phys. Lett. **91**(24), 241916 (2007).
[40] Q. Zhang, F. Guillou, A. Wahl, Y. Bréard, and V. Hardy, Appl. Phys. Lett. **96**(24), 242506 (2010).
[41] R. Wang, J. Yan, L. Xu, V. Marchenkov, S. Chen, S. Tang, and C. Yang, Solid State Commun. **151**(17), 1196–1199 (2011).
[42] A. Maiorino, M. G. Del Duca, J. Tušek, U. Tomc, A. Kitanovski, and C. Aprea, Energies **12**(10), 1871 (2019).
[43] R. L. Hadimani, J. H. B. Silva, A. M. Pereira, D. L. Schlagel, T. A. Lograsso, Y. Ren, X. Zhang, D. C. Jiles, and J. P. Araújo, Appl. Phys. Lett. **106**(3), 032402 (2015).